Impact of dry intrusions on the marine boundary layer

Eyal Ilotoviz(*), Virendra P. Ghate(**) and Shira Raveh-Rubin(*)

(*) Department of Earth and Planetary Sciences, Weizmann Institute of Science, Israel

(**) Argonne National Laboratory, US

Contact: eyal.ilotoviz@Weizmann.ac.il

Motivation and methodology

Dry air intrusions (DIs) are coherent airstreams, which descend slantwise and equatorward over thousands of kilometers from the vicinity of the tropopause to the middle and low tropospheric levels, thereby interacting with the marine boundary layer (MBL). Yet, the impact of DIs on the MBL characteristics such as the BL height, stability, BL clouds and surface fluxes are not known. The main questions we address are:

1) What synoptic systems are associated with DIs?
2) What is the impact of DIs on the surface fluxes?
3) What is the impact of DIs on the MBL characteristics such as MBL height, clouds fraction and vertical profiles of thermodynamic variables?

We combine atmospheric data from ERA Interim with measurements from the US Department of Energy Atmospheric Radiation Measurement site at Graciosa Island, Azores ($39.1^{\circ}\mathrm{N}, 28.0^{\circ}\mathrm{W}$) (Wood et al. 2015). To address the research questions, we classify the time period DJF 2016-2018 to different DI-related categories, by objective Lagrangian DI criterion (Raveh-Rubin 2017) and trailing cold front identification (Catto and Raveh-Rubin 2019).

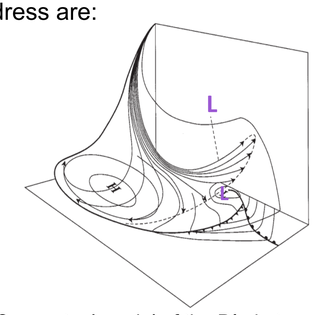

Fig. 1. Conceptual model of the DI airstream (arrows) fanning out behind the cold trailing front into the BL (Browning 1997).

Groups identification and an illustrative case study

Category	Description	Number of 6-h timesteps	% of time
Non-DIs	Climatological conditions in the absence of DIs over the Azores	649	60.5
Non-DIs fronts	Cold fronts without DIs behind	196	18.3
Pre-DIs fronts	Cold fronts with DIs behind	91	8.5
DIs	Dry intrusion events.	63 (23)	5.9
Post-DIs	24h after DI events	74	6.9
Total		1073	100

Table 1. The number of time steps for each category. The number in parenthesis presents the number of DI events. Cold trailing fronts were detected according to the gradient of wet bulb potential temperature at 850 hPa and a geometrical connection to an extratropical cyclone (Catto and Raveh-Rubin, 2019).

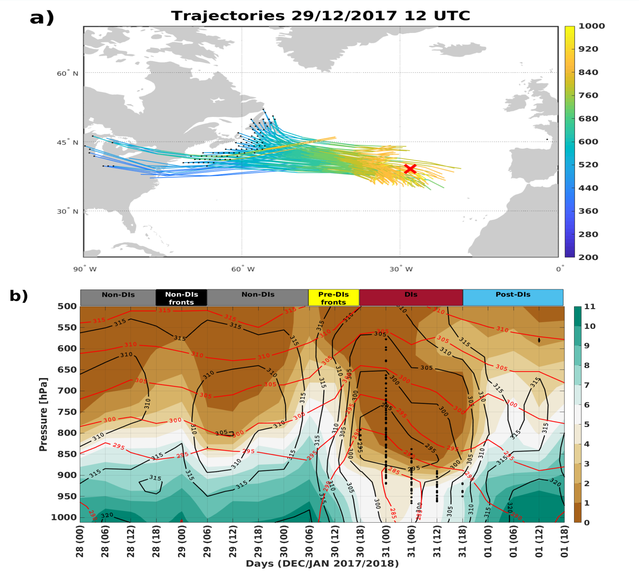

Fig. 2. A selected DI event from 28 DEC 2017 00 UTC up to 02 JAN 2018 00UTC. (a) DIs trajectories starting their descent at 12 UTC 29 DEC 2017 (black points) and lasting for 48h, colored according to their pressure (hPa). (b) Time-height cross section of specific humidity ($g\ kg^{-1}$; shaded), potential temperature (K; red contours), equivalent potential temperature (K; black contours) in the Graciosa Island (39.1^{o}N,28^{o} W). The black points mark the intersection of DI trajectories during 30-31 Dec, during the substantial drying and cooling. The upper bar illustrates the classification of the other time steps into the categories.

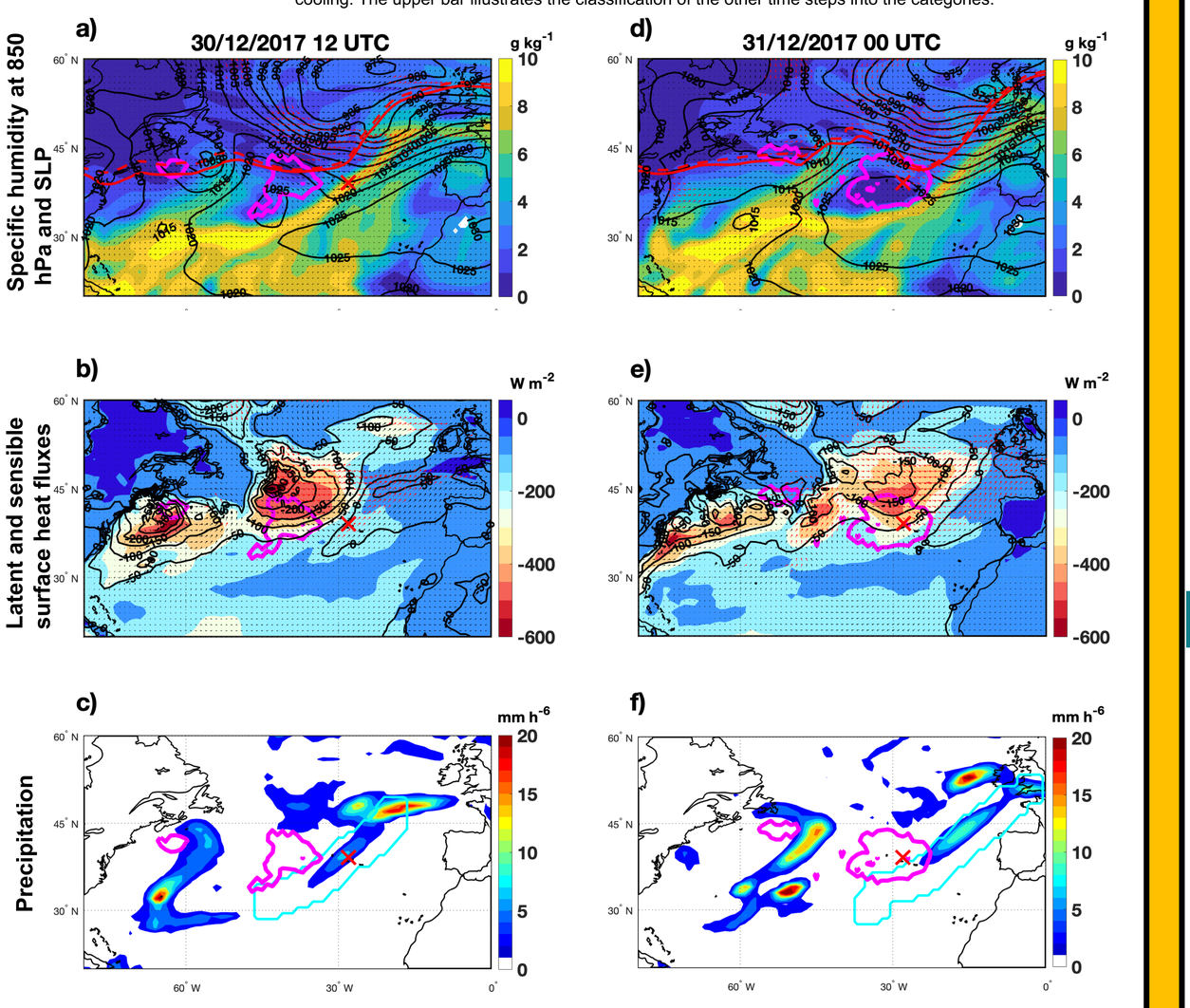

Fig. 3. Atmospheric parameters during two stages of the DI event, 12 UTC 30 Dec 2017 (pre-DI stage, left column) and 00 UTC 31 December 2017 (DI stage, right column). (a,d) Specific humidity ($g\ kg^{-1}$) at 850 hPa, SLP (black contours, at 5-hPa intervals), wind arrows at 850 hPa (red arrows for wind speeds exceeding 10 m s^{-1}). PV on the 315 K isentropic surface (2 and 3 PVU in red solid and dashed contours, respectively). (b,e) Surface latent heat flux ($W\ m^{-2}$, shaded), surface sensible heat flux (black contour, at 50 $W\ m^{-2}$ intervals). (c,f) Total accumulated precipitation over the preceding 6 h (mm). In all panels, the red 'x' marks the location of Graciosa Island, DIs outflow is encircled by the magenta contour, and the expanded cold front region is marked by the cyan contour in (c,f).

Wind directions at ENA

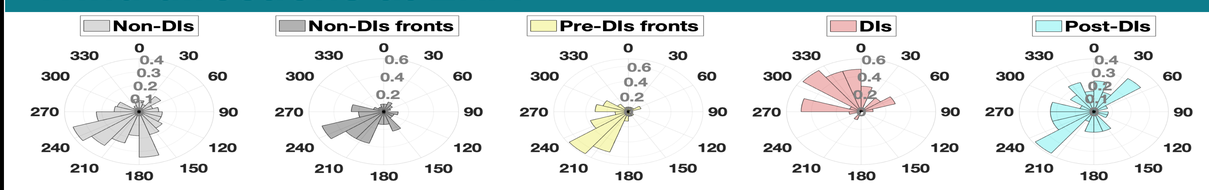

Fig. 4. Wind directions histograms from radiosondes at the lowest altitude of measurements (50 m A. G. L.) for the different categories. Northerly wind is indicated by 0 degrees.

Vertical profiles and PBL height estimations

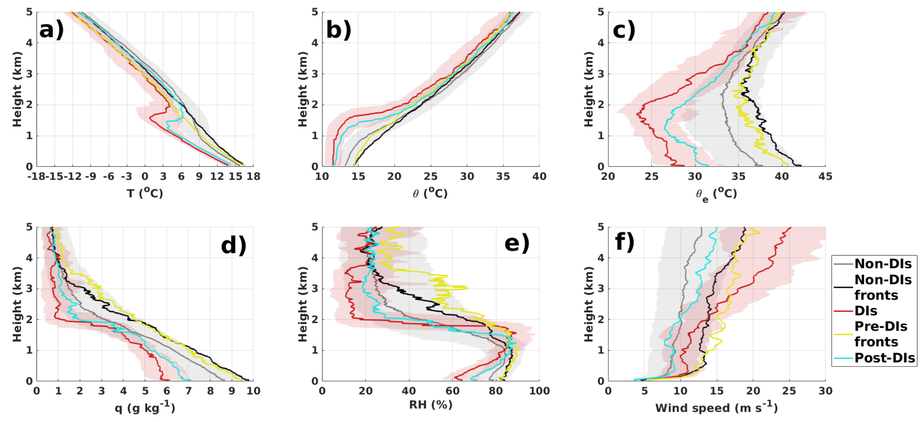

Fig. 5. Mean radiosondes vertical profiles of (a) air temperature, (b) potential temperature, (c) equivalent potential temperature, (d) water vapor mixing ratio, (e) relative humidity, and (f) horizontal wind speed. The solid lines are the median value at each height and category, and the shaded area marks the range between the to 25^{th} and 75^{th}percentiles of the Non-DIs and DIs distributions.

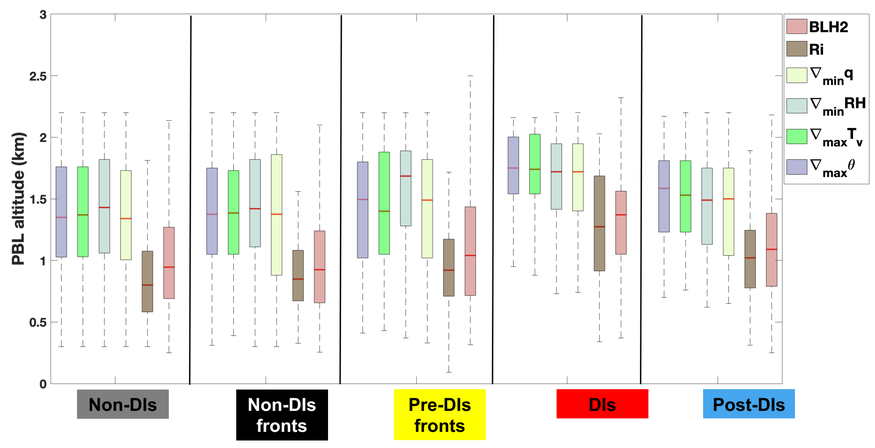

Fig. 6. PBL height (km) according to six methodologies for each category. Five definitions are based on radiosondes data: Ri uses the Richardson threshold of 0.25, four gradient definitions follow Von Engeln and Teixeira (2013). BLH2 is additionally derived from independent ceilometer data at the ENA measurement site.

The relationship between DIs, clouds and inversion properties

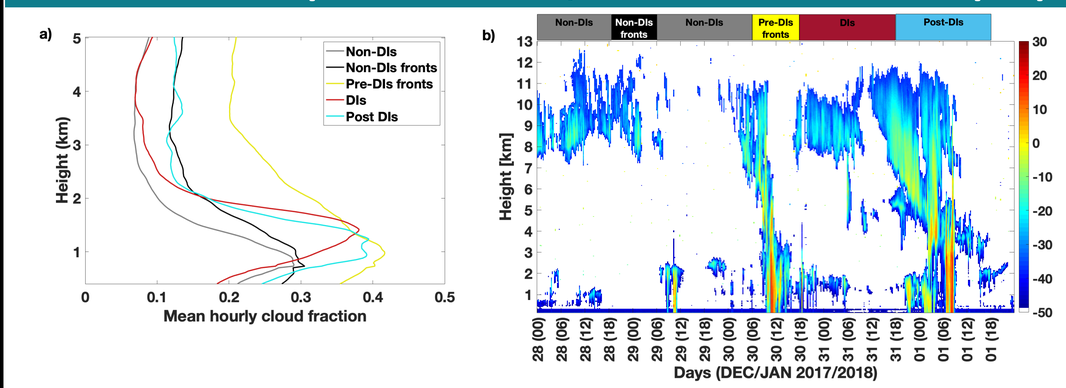

Fig. 7. (a) Mean vertical profile of hourly cloud fraction estimated from Ka-band ARM zenith, a vertical pointing radar (KAZR) for Dec-Feb from 2016 to 2018 for the different categories. (b) Retrieval of radar reflectivity for the case study 28 Dec 00 UTC 2017 to 02 Jan 00 UTC 2018 using KAZR.

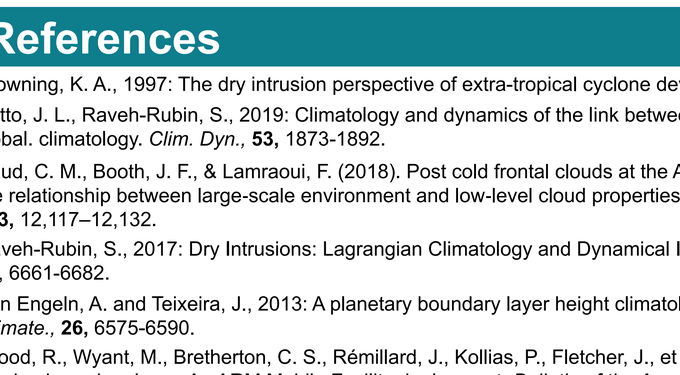

Fig. 8. Frequency histograms of (a) inversion depth and (b) temperature difference (i. e., inversion strength) across the inversion layer based on radiosondes, for all categories.

Conclusions

- Shown here by reanalysis and observational data, DIs impact the lower troposphere and MBL by sharply lowering the temperature and moisture to their lowest observed values. The arrival of DI air from the free troposphere downwards is associated with **increased MBL height and stronger inversion which is located at higher levels**, compared to other times.
- DI events are associated with trough in the upper troposphere and SLP decrease due to the passage of extratropical cyclones and their trailing front. In addition, DIs appears with **northwesterly winds** in the cold sector of the cyclone.
- A representative case study shows that DIs **enhance surface fluxes** (sensible and latent heat). Precipitation during Post-DIs are not related to post cold fronts clouds and are associated with southwesterly winds in agreement with Naud et al (2018).
- Boundary-layer clouds govern over ENA site most of the time. However, the **boundary layer stratocumulus clouds are located at an elevated altitude of 1.5 km** during DIs due to higher MBL height compared to ~1 km otherwise. Cloud fraction remains relatively high during DIs and Post-DIs compared to mean conditions.

References

Browning, K. A., 1997: The dry intrusion perspective of extra-tropical cyclone development. *Meteorol. Appl.,* **4**, 317-324.

Catto, J. L., Raveh-Rubin, S., 2019: Climatology and dynamics of the link between dry intrusions and cold fronts during winter. Part I: global. climatology. *Clim. Dyn.,* **53,** 1873-1892.

Naud, C. M., Booth, J. F., & Lamraoui, F. (2018). Post cold frontal clouds at the ARM Eastern North Atlantic site: An examination of the relationship between large-scale environment and low-level cloud properties. Journal of Geophysical Research: Atmospheres, **123,** 12,117–12,132.

Raveh-Rubin, S., 2017: Dry Intrusions: Lagrangian Climatology and Dynamical Impact on the Planetary Boundary Layer. *J. Climate.,* **30**, 6661-6682.

Von Engeln, A. and Teixeira, J., 2013: A planetary boundary layer height climatology derived from ECMWF Re-analysis data.*J. Climate.,* **26,** 6575-6590.

Wood, R., Wyant, M., Bretherton, C. S., Rémillard, J., Kollias, P., Fletcher, J., et al. 2015: Clouds, aerosols, and precipitation in the marine boundary layer: An ARM Mobile Facility deployment. *Bulletin of the American Meteorological Society.,* **96(3**), 419–440.